Lipid Droplets Mediate Salt Stress Tolerance in *Parachlorella kessleri*[1]

Zaizhi You,[a,b,c] Qi Zhang,[a,b,c] Zhou Peng,[a,b,c] and Xiaoling Miao[a,b,c,2,3]

[a]State Key Laboratory of Microbial Metabolism, School of Life Sciences and Biotechnology, Shanghai Jiao Tong University, Shanghai 200240, China

[b]Joint International Research Laboratory of Metabolic and Developmental Sciences, Shanghai Jiao Tong University, Shanghai 200240, China

[c]Biomass Energy Research Center, Shanghai Jiao Tong University, Shanghai 200240, China

Microalgae are known to respond to salinity stress via mechanisms that include accumulation of compatible solutes and synthesis of antioxidants. Here, we describe a salinity-tolerance mechanism mediated by lipid droplets (LDs). In the alga *Parachlorella kessleri* grown under salt-stress conditions, we observed significant increases in cell size and LD content. LDs that were closely grouped along the plasma membrane shrank as the plasma membrane expanded, and some LDs were engulfed by vacuoles. Transcriptome analysis showed that genes encoding lysophospholipid acyltransferases (LPLATs) and phospholipase A2 were significantly up-regulated following salt stress. Diacylglycerol kinase and LPLAT were identified in the proteome of salt-induced LDs, alongside vesicle trafficking and plastidial proteins and histone H2B. Analysis of fatty acid composition revealed an enrichment of C18:1 and C18:2 at the expense of C18:3 in response to salt stress. Pulse-chase experiments further suggested that variations of fatty acid composition were associated with LDs. Acetate stimulation research further confirmed a positive role of LDs in cell growth under salt stress. These results suggest that LDs play important roles in salt-stress tolerance, through harboring proteins, participating in cytoplasmic component recycling, and providing materials and enzymes for membrane modification and expansion.

Salt stress impairs plant growth, and salt contamination of soil increasingly poses serious problems for agriculture (Mastrobuoni et al., 2012). Microalgal species serve as good models for research on plant salinity stress responses due to their shared physiological and biochemical reactions (Harris, 2001; Hicks et al., 2001). Furthermore, microalgae are of interest for the green bioenergy, animal feed, and human food industries due to their high oil productivity, high levels of protein, and high content of valuable natural products such as carotenoids (Pulz and Gross, 2004). Large-scale cultivation of microalgae in the future will have to be carried out in seawater or brackish waters because of limitations in freshwater supply (Borowitzka and Moheimani, 2013; Chisti, 2013). Thus, a comprehensive understanding of the adaptation strategies of green algae to salt stress is critical.

In general, salt stress results in ionic imbalances, osmotic stress, and oxidative damage. To survive under these conditions, microalgae respond and adapt with complex mechanisms including exclusion of harmful ions via a variety of transport systems, accumulation of compatible solutes, and synthesis of antioxidants and antioxidant enzymes responsible for reactive oxygen species (ROS) scavenging (Noctor and Foyer, 1998; Borowitzka et al., 2016). Active transporters such as Na^+/H^+ antiporters and Na^+-ATPase contribute to maintaining low, nontoxic internal Na^+ contents (Wang et al., 2002; Dibrova et al., 2010). In terms of osmotic equilibrium, the salt tolerance level correlates with compatible solutes (Hagemann, 2011). Pro metabolism is significantly up-regulated in *Chlamydomonas reinhardtii* (hereafter *Chlamydomonas*) under salt stress, potentially providing resistance to salt stress in this species (Mastrobuoni et al., 2012). The -omics approaches have revealed a global picture of the salt-stress response process in microalgae. Transcriptomic studies have revealed that genes encoding metal transporters, Pro metabolism, and antioxidants (thioredoxins and glutaredoxin) are all significantly up-regulated in *Chlamydomonas* under salt stress (Perrineau et al., 2014). Moreover, proteomic analysis showed that antioxidant enzymes (ascorbate peroxidase and NADPH-dependent thioredoxin reductase), as well as heat shock proteins and chaperones, which can aid in protein folding, appear

[1]This work was supported by the National Natural Science Foundation of China (41476122) and by the National High Technology Research and Development Program (863 Program) of China (2013AA065805).

[2]Author for contact: miaoxiaoling@sjtu.edu.cn.

[3]Senior author.

The author responsible for distribution of materials integral to the findings presented in this article in accordance with the policy described in the Instructions for Authors (www.plantphysiol.org) is: Xiaoling Miao (miaoxiaoling@sjtu.edu.cn).

Z.Y. and Q.Z. performed experiments; Z.Y. and X.M. designed experiments; Z.Y., Q.Z., Z.P., and X.M. analyzed data; Z.Y. wrote the article with contributions from X.M., who supervised the project.

www.plantphysiol.org/cgi/doi/10.1104/pp.19.00666

following salt stress (Yokthongwattana et al., 2012). Taken together, these studies indicate that the salinity stress response is comprehensive and involves global metabolic changes.

Under salt stress, microalgae accumulate neutral lipids, mainly triacylglycerols (TAGs), in specialized organelles known as lipid droplets (LDs; Murphy, 1993; Thompson, 1996; Wältermann and Steinbüchel, 2005; Sibi et al., 2016). LDs consist of a core of TAGs and/or sterol esters that are coated by a phospholipid (PL) monolayer and a unique set of proteins (Murphy, 1993; Wältermann and Steinbüchel, 2005). LDs are conserved from bacteria to mammals (Murphy, 2012). Under iron starvation, TAG accumulation and the appearance of LDs were observed, but there was no net synthesis of fatty acids (FAs) in algae, suggesting that LDs serve as storage for acyl chains (Urzica et al., 2013). These acyl chains are released from TAGs and used for membrane lipid synthesis when environmental conditions become favorable again. Under nitrogen deprivation, lysophospholipid acyltransferase (LPLAT) was found in the LD proteome of *Chlamydomonas*, suggesting that LDs may be sites of acyl exchange (Nguyen et al., 2011). Based on data from the LD proteome and evidence in other organisms, microalgal LDs are postulated to play multiple roles in processes such as cell signaling and FA trafficking (Nguyen et al., 2011). However, it is currently poorly understood if microalgal LDs play roles in response to salt stress.

In this work, we used *Parachlorella kessleri* to demonstrate that microalgal cells growing under salt stress significantly increase their size and LD content, implying that these changes are salt-stress responses. Furthermore, using phenotypic assays, RNA sequencing, confocal microscopy, and transmission electron microscopy, we examined transcriptomes and cellular anatomy to dissect the functional role of LDs in this phenomenon. We propose that LDs play an important role under salinity stress.

RESULTS

Cell Size and Lipid Content of *P. kessleri* under Salt Stress

When *P. kessleri* cells were cultivated in medium with either 0 or 350 mM NaCl concentration, significant differences were found in cell size (Fig. 1A). Cells treated with 350 mM NaCl for 7 d displayed a sharp increase in size. Differential interference contrast (DIC) images showed that larger salt-treated cells were not a group of dividing cells (Supplemental Fig. S1). We further measured the cell volume of thousands of individual cells per population using a Coulter Counter. Control conditions (0 mM NaCl) produced a uniform cell size distribution (~150 μm^3), whereas salt stress resulted in variations in cell size ranging from 80 to 2,000 μm^3 (Fig. 1B). Size distribution analysis indicated a distinct shift away from smaller cells (~150 μm^3) under salinity, with enrichment in a specific population centered around 1,000 μm^3 (Fig. 1B). The cell volume increased about 6.7-fold.

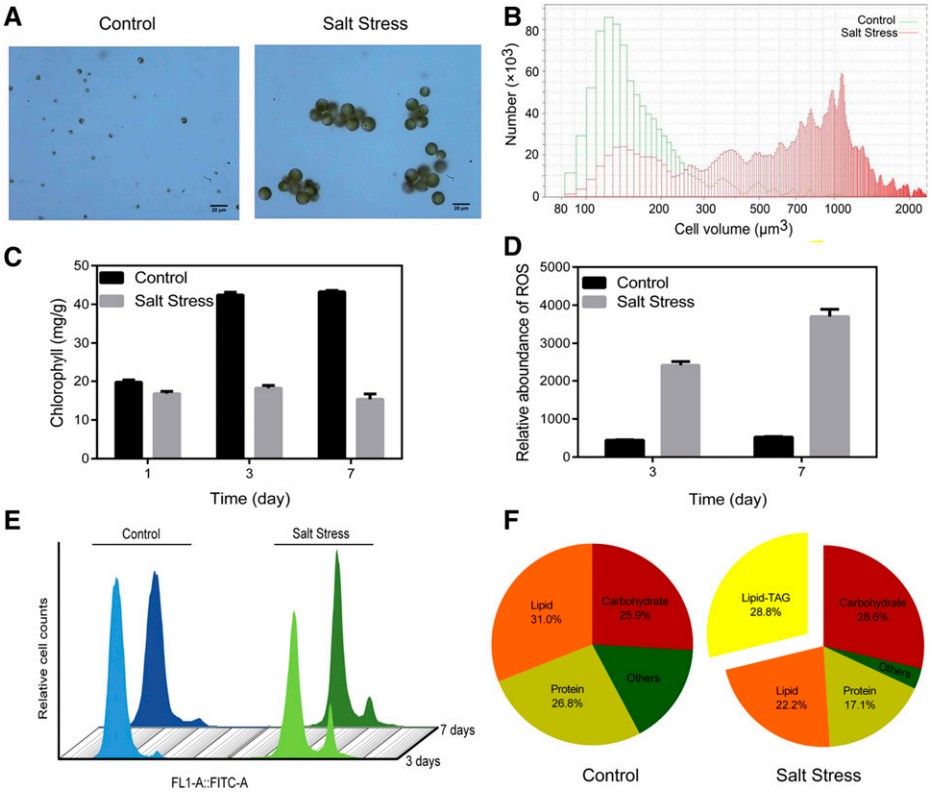

Figure 1. Effect of salt stress on the cell morphology, physiology, and biochemical composition of *P. kessleri*. A, Cell morphology under control (0 mM NaCl) and salt-stress (350 mM NaCl) conditions was examined by microscopy. B, Cell volume population distribution comparison between the two experimental conditions. C, Chlorophyll content in response to salt stress in cells at 1, 3, and 7 d. D, Relative abundance of ROS in salt-treated and untreated cells at 3 and 7 d. Values are means ± SD of three independent biological replicates. E, Flow cytometry analysis of percentage of death cell under control and salt-stress conditions at 3 and 7 d. F, Biochemical composition of *P. kessleri* cultivated in Tris-acetate phosphate (TAP) medium under control and salt-stress conditions. The content is based on dry cell weight (%).

Salt-induced hypertrophy is related to NaCl sensitivity (Takouridis et al., 2015). Such large morphological alterations suggest that cells are likely facing a survival threat and may use multiple strategies to overcome this. The chlorophyll content was reduced by 1.8-fold after 7 d of salt treatment compared with that of untreated cells (Fig. 1C), implying that there was chloroplast degradation and that the stressed cells had some degree of damage. Moreover, significantly higher ROS contents in salt-treated cells were observed (Fig. 1D), suggesting that salt stress caused ROS accumulation leading to cellular damage in *P. kessleri*. However, we observed that the percentage of dead cells (the first peak represents live cells and the second represents dead cells) was lower in cultures treated with salt for 7 d than in cultures treated for 3 d (Fig. 1E). These results suggest that salt stress may cause cellular damage and that salt-induced cell enlargement might be associated with increased cell survival.

To examine which cellular component was responsible for increased cell size, the biochemical composition of dry cell weight was examined. Salt stress resulted in a decrease in cellular protein content from 26.8% to 17.1% dry cell weight, whereas lipid content increased significantly from 31% to 51% dry cell weight (Fig. 1F). Salt treatment led to considerable accumulation of TAGs, increasing from 0% to 28.8% dry cell weight (Fig. 1F). A slight increase (from 25.9% to 28.6% dry cell weight) in carbohydrates was also observed. In terms of energy storage, both starch and TAG accumulation constitute functional redundancy for cells facing a survival threat as a result of salinity. As TAG accumulation is tightly associated with the formation of LDs (Jolivet et al., 2013) and LDs have emerged as a central hub involved in multiple previously unanticipated cellular functions, we speculate that, besides serving as storage for energy homeostasis, LDs may play other roles in response to salt stress and contribute to increased cell survival.

Transcriptional Characteristics in Response to Salt Stress

To understand the molecular basis of the *P. kessleri* salinity stress response, we carried out transcriptome sequencing and analyzed differently expressed genes. Genes encoding enzymes related to development include cell division cycle protein48 homolog (cdc48), cytokinesis protein sepA, anaphase-promoting complex subunit (APC), and mitogen-activated protein kinases homolog1 (MAPK; Table 1). Genes encoding cytokinesis protein sepA, which is involved in cytoplasmic division, and cdc48, whose transcription occurs during the cell division cycle, were down-regulated under salt stress. Moreover, genes encoding APC, which is involved in entry into anaphase and exit from mitosis, and MAPK, which is responsible for cell cycle arrest allowing cells to survive upon stress in yeast (Correia et al., 2010), were significantly up-regulated. These results suggest that cell division processes ceased during salt stress. Based on the results of DIC image analysis (Supplemental Fig. S1), as well as the observed expression changes of development genes, enlarged

Table 1. *Differentially expressed genes involved in development, Pro metabolism, antioxidant activity, and lipases in* P. kessleri *during salt stress*

All presented fold changes (LogFC) are statistically significant, $q < 0.05$.

Enzyme Encoded	Gene Seq_id	LogFC
Development		
Cell division cycle protein48 homolog (cdc48)	TRINITY_DN5222_c2_g7	−1.38
Cytokinesis protein sepA	TRINITY_DN5103_c0_g4	−1.37
Anaphase-promoting complex subunit (APC)	TRINITY_DN4003_c0_g2	1.52
MAPK homolog1 (MAPK)	TRINITY_DN3213_c0_g1	2.11
Pro metabolism		
Glu 5-kinase (EC 2.7.2.11)	TRINITY_DN4465_c0_g1	2.65
Pyrroline 5-carboxylate reductase (EC 1.5.1.2)	TRINITY_DN4877_c3_g1	1.79
Asp transaminase (EC 2.6.1.1)	TRINITY_DN5053_c1_g1	1.31
	TRINITY_DN5867_c1_g2	2.44
Pro hydroxylase (EC 1.14.11.2)	TRINITY_DN5731_c1_g3	−3.64
	TRINITY_DN6027_c1_g3	−3.61
	TRINITY_DN3673_c0_g1	−1.52
Antioxidant activity		
Thioredoxin	TRINITY_DN4480_c2_g5	2.65
Glutaredoxin	TRINITY_DN3285_c0_g1	1.74
	TRINITY_DN3664_c0_g1	1.58
Catalase (EC 1.11.1.6)	TRINITY_DN5788_c1_g5	3.73
Lipases		
Phospholipase A1 (PLA1; EC 3.1.1.32)	TRINITY_DN5906_c1_g2	−2.92
Phospholipase A2 (PLA2; EC 3.1.1.4)	TRINITY_DN5505_c1_g4	1.98
	TRINITY_DN5911_c1_g2	1
	TRINITY_DN5912_c0_g4	−1.36

P. kessleri cells caused by salt stress are likely giant cells rather than a group of dividing cells.

The most common strategy used by microalgae to survive and grow in saline environments is the accumulation of compatible solutes, including Suc, trehalose, glucosylglycerate, isofloridoside, Gly betaine, and Pro (Borowitzka et al., 2016). Pro is accumulated in cells of diatoms and salt-treated green algae as the main compatible solute (Andreas et al., 2007; Bromke et al., 2013; Borowitzka et al., 2016). The primary response of *P. kessleri* to salt stress was similar to that of green algae. As expected, genes encoding Glu 5-kinase and pyrroline 5-carboxylate synthetase, two critical enzymes needed to convert Glu into Pro, were highly up-regulated after salt exposure. In addition, genes associated with Glu synthesis were also up-regulated, resulting in an increase in precursor supply for Pro synthesis. By contrast, we detected a significant decrease in expression of the gene encoding Pro hydroxylase, an enzyme related to Pro degradation. Besides accumulating compatible solutes, microalgae also synthesize antioxidant enzymes such as superoxide dismutase and catalase (CAT) to defend against high levels of ROS induced by salt stress (Fig. 1D). Several genes involved in ROS scavenging were significantly up-regulated by salt treatment, including gene families encoding CAT, thioredoxins, and glutaredoxin. The fold changes in expression of the genes mentioned above are presented in Table 1. These data indicate that *P. kessleri* enhances antioxidant defense and accumulates compatible solutes to counteract oxidative and osmotic stress caused by saline growth conditions.

Analysis of starch metabolism pathways showed that the majority of genes governing starch biosynthesis were up-regulated in salt-treated cells (Fig. 2A). On the other hand, genes encoding enzymes associated with starch degradation, including α-amylase, β-amylase, isoamylase, and starch phosphorylase, were strongly repressed under salt stress. These data suggest that both enhanced synthesis and repressed degradation contribute to starch accumulation observed under salt-stress conditions.

We focused on genes related to lipid metabolism because of their relevance to the cell size increase. Although the expression of genes coding for FabF and FabH was up-regulated, the gene encoding acetyl-coenzyme A carboxylase (ACCase), which catalyzes the first committed step of FA biosynthesis, was repressed in salt-treated cells (Fig. 2B). Overexpression of ACCase does not increase lipid content in diatoms (Dunahay et al., 1995) or plants (Roesler et al., 1997). Up-regulation of acetyl-coenzyme A synthetase (ACS) in *Chlorella desiccata* (Avidan and Pick, 2015) or ATP:citrate lyase in the yeast *Yarrowia lipolytica*, two enzymes responsible for acetyl-CoA production, results in a large increase in lipid yields (Blazeck et al., 2014). A buildup of acetyl-CoA contributes more toward lipid accumulation than the activity of ACCase (Tan and Lee, 2016). In our study, although the gene for ACS was strongly repressed by salt stress, exogenously available acetate could still be used for acetyl-CoA biosynthesis when acetate was present in the medium. Highly active glycolysis also contributed to the generation of acetyl-CoA. Down-regulation of citrate synthase and 3-hydroxy-3-methylglutaryl-CoA synthase shunted acetyl-CoA away from the tricarboxylic acid cycle and ketone body synthesis (Fig. 2C). Therefore, more acetyl-CoA was channeled into FA synthesis. Additionally, four of the five genes involved in FA degradation (the typical β-oxidation pathway for saturated FAs) were down-regulated by salt stress, showing that increased FA supply preceded lipid accumulation (Fig. 2D).

During salt stress, there was up-regulation of the genes for glycerol-3-phosphate acyltransferase, which catalyzes the acylation of glycerol-3-phosphate to produce lysophosphatidic acid, and lysophosphatidic acid acyltransferase (LPAAT), which leads to the formation of phosphatidic acid (PA), whereas there was down-regulation of the genes for phosphatidate phosphatase converting PA into diglycerides and diacylglycerol *O*-acyltransferase catalyzing the formation of TAGs (Fig. 2E). These results suggested that fatty acyl chains from PA might provide a greater contribution to membrane biogenesis than TAG. Triacylglycerol lipase, lipase (class 3), and putative phospholipase A1, involved in the release of FAs from TAGs, were all repressed in gene expression during salt stress (Fig. 2E; Table 1). These findings suggest that the observed increase in TAGs in response to salt treatment is mainly due to inhibited TAG degradation.

Genes encoding LPLATs, which are involved in PL remodeling, were highly induced by salt stress in *P. kessleri* (Fig. 2E). Phospholipids are remodeled through deacylation and reacylation processes, defined as the Lands cycle (Lands, 1958), also termed acyl editing. The LPLAT-remodeling enzymes include LPAAT, lyosphosphatidylglycerol acetyltransferase, lysophosphatidylcholine acyltransferase (LPCAT), lyosphosphatidylethanolamine acyltransferase, lyosphosphatidylserine acyltransferase, and lyosphosphatidylinositol acyltransferase, based on their substrate specificities (Shindou and Shimizu, 2009). Phospholipase A2 (PLA2) is another remodeling enzyme in the Lands cycle, which hydrolyzes fatty acyl chains at the *sn*-2 position of PLs (Lands, 2000; Shimizu et al., 2006). Saturated FAs are found frequently at the *sn*-1 position of PLs, whereas unsaturated FAs, usually found at the *sn*-2 position, are esterified mainly through the remodeling process (Waku and Nakazawa, 1972; Yamashita et al., 1997; Lands, 2000). Of three putative PLA2 (*sn*-2-specific phospholipase) genes found in salt-treated *P. kessleri* cells, two were up-regulated and one was down-regulated, whereas the gene for phospholipase A1 (*sn*-1-specific phospholipase) was sharply down-regulated (Table 1). The results of this study and previous work on LPLAT genes were confirmed using reverse transcription quantitative PCR (RT-qPCR; Supplemental Fig. S2; Supplemental Table S1). Genes

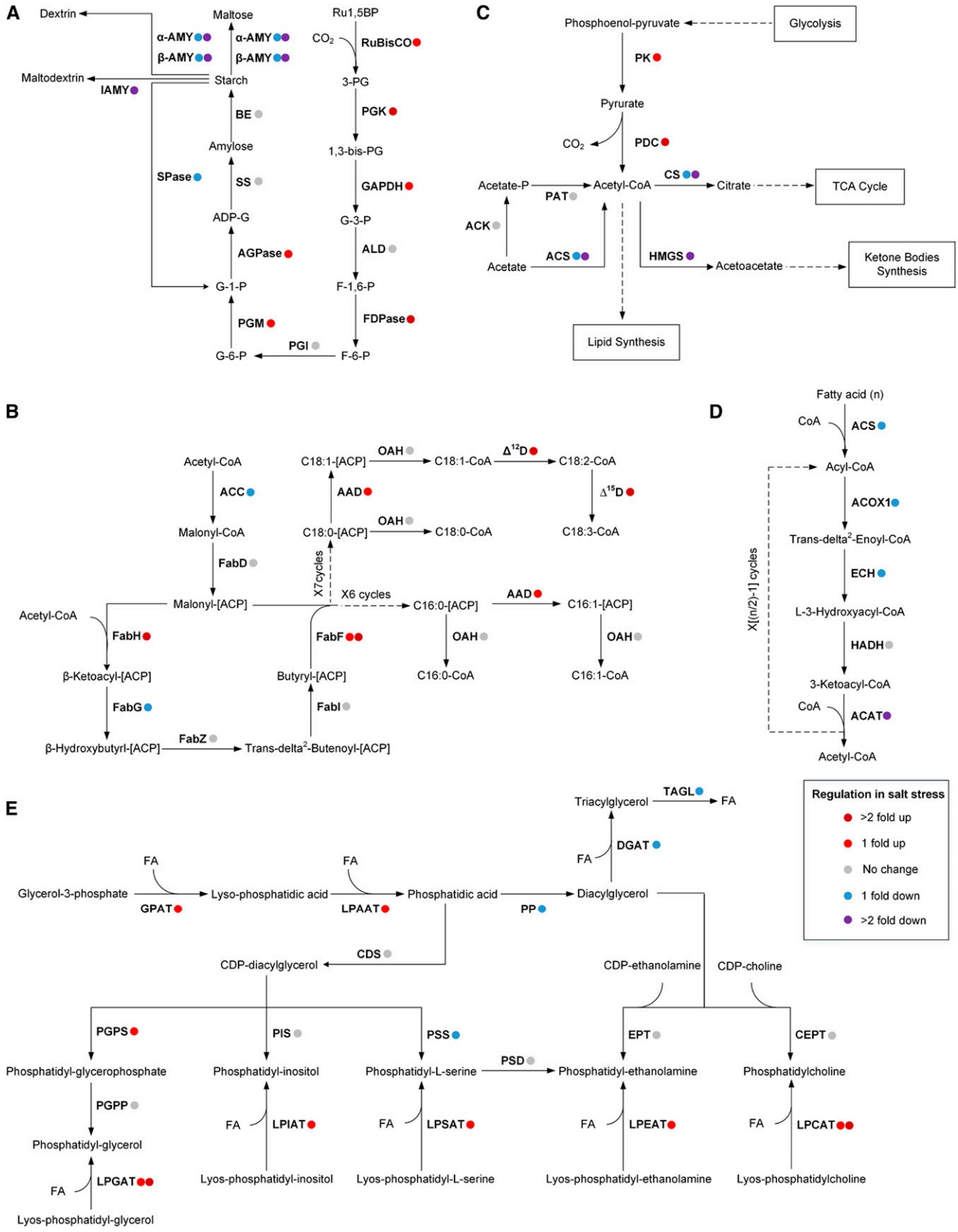

for acyl-ACP desaturase (AAD), which introduces one double bond to C16:0/C18:0; Δ-12 desaturase, which converts C18:1 to C18:2; and Δ-15 desaturase, which further desaturates C18:2 to form 18:3, were significantly up-regulated, implying that variations in FA composition occurred (Fig. 2B). Taking these data together, we speculate that LPLAT, PLA2, and desaturase enzymes participate in membrane reorganization during salt stress. Given that LDs are connected to diverse cellular processes such as membrane and FA trafficking and lipid biosynthesis, this reorganization may be related to LDs.

LD Distribution in Salt-Treated Cells

To investigate whether LDs were involved in membrane remodeling, the subcellular localization of the LDs in *P. kessleri* cells was detected using Nile Red staining. There was a large difference in LDs between the cultures with NaCl and those without NaCl. After salt exposure for 1 d, LDs were observed, whereas they were absent in untreated cells throughout the cultivation period, consistent with the previous analysis of cellular biochemical composition (Fig. 3, A–H; Supplemental Fig. S3). The number of LDs increased and the relative volume of chloroplasts decreased as cultivation under salt proceeded (Fig. 3, I–T). In some cases, chlorophyll fluorescence colocalized with that of LDs (Fig. 3, O, P, R, and S, white arrows), suggesting that components of the chloroplast were converted into LDs as the chloroplast degraded. Many small LDs of a similar size (~0.4 μm in diameter) were grouped along the cell periphery (Fig. 3, I, L, O, and R). Such distribution of salt-induced LDs implies that they are functionally linked to plasma membrane reorganization. To further test this hypothesis, we examined variations in FA composition of salt-treated and untreated *P. kessleri* cells.

Variations of FA Composition in Response to Salt Stress

FA composition of *P. kessleri* cells grown under both control and salt-stress conditions, as well as their LDs, are shown in Table 2. Salt stress resulted in an increase in C18:1 from 0% to 15.58% of total fatty acids (TFA) and C18:2 from 30.54% to 56.02% of TFA, consistent with the observed overexpression of genes encoding AAD and Δ-12 desaturase (Fig. 2B). Although Δ-15 desaturase was also up-regulated, the content of C18:3 decreased from 25.27% to 0.07% of TFA. This phenomenon was also observed in *Neochloris oleoabundans* cells cultivated under nitrogen-starvation conditions (Rismani-Yazdi et al., 2012). In addition to the ω-3 FA desaturase domain, the putative Δ-15 desaturase also contains a Δ-12-FADS-like domain, raising the possibility that it functions as a Δ-12 desaturase under salt stress, thus resulting in the decrease of C18:3. The contents of C18:3 in membrane lipids were further analyzed using ultra-HPLC (UHPLC). As shown in Figure 4A, the proportion of C18:3 in PL was reduced under salt stress following 7 d of cultivation. Although the proportion of C18:3 under control conditions also decreased, the differences were not

Figure 2. (*Continued.*)
Differential expression of selected genes to salt stress in *P. kessleri*. A, Starch metabolism. B, FA metabolism. C, Acetyl-CoA metabolism. D, β-Oxidation. E, Glycerolipid and glycerophospholipid metabolism. Pathways were reconstructed based on the de novo assembly and quantitative annotation of the *P. kessleri* transcriptome. A, Encoded enzymes include Rubisco (EC 4.1.1.39); PGK, phosphoglycerate kinase (EC 2.7.2.3); GAPDH, glyceraldehyde 3-phosphate dehydrogenase (EC 1.2.1.13); ALD, Fru-1,6-bisphosphate aldolase (EC 4.1.2.13); FDPase, Fru-1,6-bisphosphate 1-phosphohydrolase (EC 3.1.3.11); PGI, phosphoglucose isomerase (EC 5.3.1.9); PGM, phosphoglucomutase (EC 5.4.2.2); AGPase, ADP-Glc pyrophosphorylase (EC 2.7.7.27); SS, starch synthase (EC 2.4.1.21); BE, 1,4-α-glucan branching enzyme (EC 2.4.1.18); α-AMY, α-amylase (EC 3.2.1.1); β-AMY, β-amylase (EC 3.2.1.2); SPase, starch phosphorylase (EC 2.4.1.1); and IAMY, isoamylase (EC 3.2.1.68). B, Encoded enzymes include PK, pyruvate kinase (EC 2.7.1.40); PDC, pyruvate dehydrogenase complex (EC 1.2.4.1); ACS, acetyl-CoA synthase (EC 6.2.1.1); ACK, acetate kinase (EC 2.7.2.1); PAT, phosphate acetyltransferase (EC 2.3.1.8); CS, citrate synthase (EC 2.3.3.1); and HMGS, 3-hydroxy-3-methylglutaryl-CoA synthase (EC 2.3.3.10). C, Encoded enzymes include ACC, acetyl-CoA carboxylase (EC 6.4.1.2); FabD, malonyl-CoA ACP transacylase (EC 2.3.1.39); FabH, β-ketoacyl-ACP synthase III (EC 2.3.1.180); FabF, β-ketoacyl-ACP synthase I/II (EC 2.3.1.41); FabG, β-ketoacyl-ACP reductase (EC 1.1.1.100); FabZ, β-hydroxyacyl-ACP dehydrase (EC 4.2.1.56); FabI, enoyl-ACP reductase (EC 1.3.1.9); AAD, acyl-ACP desaturase (EC 1.14.19.2); OAH, oleoyl-ACP hydrolase (EC 3.1.2.14); Δ12D, Δ12(ω6)-desaturase (EC 1.4.19.6); and Δ15D, Δ15(ω3)-desaturase (EC 1.4.19.-). D, Encoded enzymes include ACS, acyl-CoA synthase (EC 6.2.1.3); ACOX1, acyl-CoA oxidase (EC 1.3.3.6); ECH, enoly-CoA hydratase (EC 4.2.1.17); HADH, 3-hydroxyacyl-CoA dehydrogenase (EC 1.1.1.35); and ACAT, acetyl-CoA C-acetyltransferase (EC 2.3.1.16 and 2.3.1.9). E, Encoded enzymes include GPAT, glycerol-3-phosphate *O*-acyltransferase (EC 2.3.1.15); LPAAT, lysophosphatidic acid acyltransferase (EC 2.3.1.51); PP, phosphatidate phosphatase (EC 3.1.3.4); DGAT, diacylglycerol *O*-acyltransferase (EC 2.3.1.20); TAGL, triacylglycerol lipase (EC 3.1.1.3); CDS, CDP-diglyceride synthase (EC 2.7.7.41); PGPS, phosphatidylglycerolphosphate synthase (EC 2.7.8.5); PGPP, phosphatidylglycerolphosphate phosphatase (EC 3.1.3.27); PIS, phosphatidylinositol synthase (EC 2.7.8.11); PSS, phosphatidylserine synthase (EC 2.7.8.8); PSD, phosphatidylserine decarboxylase (EC 4.1.1.65); EPT, diacylglycerol ethanolaminephosphotransferase (EC 2.7.8.1); CEPT, diacylglycerol cholinephosphotransferase (EC 2.7.8.2); LPGAT, lysophosphatidylglycerol acetyltransferase; LPCAT, lysophosphatidylcholine acyltransferase; LPEAT, lysophosphatidylethanolamine acyltransferase; LPSAT, lysophosphatidylserine acyltransferase; and LPIAT, lysophosphatidylinositol acyltransferase. Dashed arrows denote reaction(s) for which the enzymes are not shown. All presented fold changes are statistically significant, $q < 0.05$.

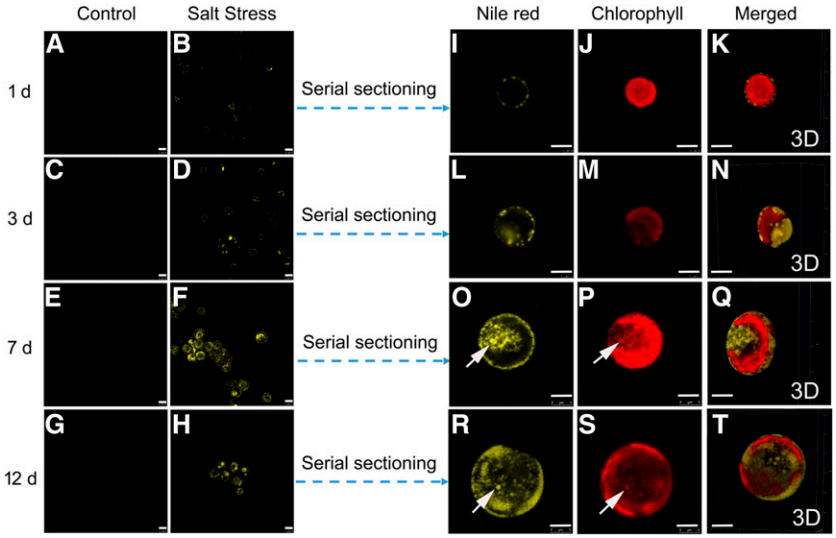

Figure 3. Visualization of LDs and chlorophyll autofluorescence by confocal microscopy. A to H, Nile Red-stained *P. kessleri* cells cultivated under control (left column) and salt-stress (right column) conditions for 1, 3, 7, and 12 d. I to T, Serial sectioning images of a Nile Red-stained salt-treated cells after 7 and 12 d. LDs appear yellow (left column) and chlorophyll fluorescence appears red (middle column). The right column (Merged) presents merged images of LDs and chlorophyll fluorescence. White arrows represent a single LD. Bars = 10 μm in A to H and 5 μm in I to T.

significant. In addition, the proportion of C18:3 in phosphatidylcholine increased under control conditions and decreased under salt stress (Fig. 4B). These results suggest that FA composition of membrane lipids also changed under salt stress. A decrease in unsaturated FAs could reduce plasma membrane permeability and fluidity, thus contributing to salt tolerance (Mansour et al., 2015). Furthermore, polyunsaturated FAs such as C18:3 are susceptible to ROS-induced peroxidation that can damage membrane PLs as well as nonlipid macromolecules (Bailey et al., 2015). Therefore, the increase of C18:1 and C18:2 and the decrease of C18:3 may contribute to not only maintaining appropriate membrane fluidity but also reducing membrane peroxidation. More importantly, FA composition of LDs is similar to that of salt-treated *P. kessleri* cells, and C18:3 was found in LDs (Table 2). This result suggests that LDs dynamically interact with other structures of the cell and participate in membrane reorganization.

Pulse-Chase Imaging of Lipid Dynamics in Response to Salt Stress

We investigated membrane lipid dynamics with Bodipy FL C12 using microscopy as well as thin-layer chromatography (TLC) plates. Bodipy-labeled FA was incorporated into lipids and emitted green fluorescence, whereas the chloroplast emitted red autofluorescence. Initially, the whole cell appeared to emit green fluorescence, implying that different classes of lipids contained fluorescent FA (Fig. 4C, 0 d). Under control conditions, this distribution of fluorescent FA remained the same. However, under salt stress, fluorescent FA gradually distributed to the cell periphery, where LDs were initially formed. Moreover, fluorescent FAs were also found in LDs (TAGs; Fig. 4C; Supplemental Figs. S4 and S5). Accompanied by the increase of TAGs (LDs) under salt stress, the amounts of monogalactosyldiacylglycerol (MGDG) and digalactosyldiacylglycerol, which are the most abundant lipids in photosynthetic membranes, decreased by 55% and 63%, respectively (UHPLC data). TLC plates also showed that the amount of fluorescent FA incorporated into MGDG decreased (Supplemental Fig. S5). An enzyme that cleaves FAs from MGDG has been identified in *Chlamydomonas*, implying a possible mechanism for recycling of FAs (Li et al., 2012a). Chloroplast glycolipids appear to be broken down in both *Chlorella* sp. and *Nannochloropsis* sp. in response to nitrogen deprivation, which are then recycled for TAG synthesis (Martin et al., 2014). The increase of LDs and decrease of

Table 2. *FA composition of* P. kessleri *cells and their LDs during salt stress*

Data are means ± SD of three independent biological replicates. nd, Not detected.

FA	Control (Cells)	Control (LDs)	350 mM NaCl (Cells)	350 mM NaCl (LDs)
16:0	15.37 ± 0.36	nd	15.06 ± 0.42	12.58 ± 0.29
16:1	nd	nd	1.22 ± 0.09	1.32 ± 0.03
16:2	4.94 ± 0.20	nd	1.42 ± 0.03	0.97 ± 0.02
16:3	1.65 ± 0.08	nd	nd	nd
18:0	0.24 ± 0.02	nd	3.36 ± 0.76	2.45 ± 0.02
18:1	nd	nd	15.58 ± 2.99	25.85 ± 0.29
18:2	30.54 ± 1.98	nd	56.02 ± 3.79	49.61 ± 0.42
18:3	25.27 ± 1.20	nd	0.07 ± 0.02	0.08 ± 0.03
Other	21.99	nd	7.34	6.19

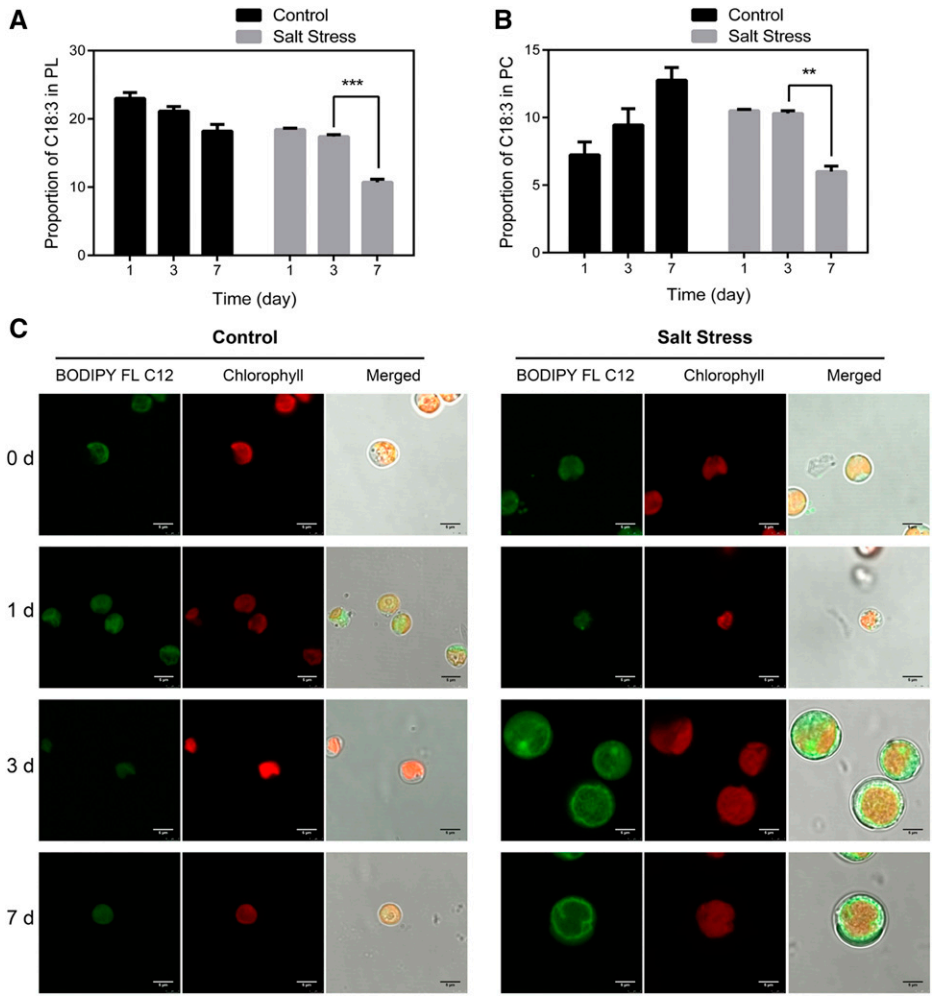

Figure 4. Dynamic variations of FAs in *P. kessleri* cells under salt stress for 1, 3, and 7 d. A, C18:3 in PL. B, C18:3 in phosphatidylcholine (PC). Values are means ± SD of three replicates. Student's *t* test was performed to determine statistically significant differences: **, $P < 0.01$ and ***, $P < 0.001$. C, Pulse-chase imaging of fluorescent FAs. Fluorescent FAs appear green (left column) and chlorophyll fluorescence appears red (middle column). The right column (Merged) presents merged images of fluorescent FAs and chlorophyll fluorescence. Bars = 5 μm.

chloroplast glycolipids under salt stress suggest that membrane lipid turnover also contributes to LD (TAG) production and LD participation in dynamic remodeling of membrane lipids.

The fluorescent FA presented in almost all lipid classes except for TAGs, which were absent or very low in content under control conditions. Notably, fluorescent FA in PL significantly decreased and TAGs with fluorescent FA were produced after 1 d of salt stress. However, fluorescent FA in PL increased after 3 d of salt stress, implying that PL underwent dynamic remodeling and that this remodeling was associated with LDs (TAGs; Supplemental Fig. S5).

Protein Identification of LDs Accumulated during Salt Exposure

To gain further insights into LD function under salt stress, a proteomic analysis of LDs isolated from salt-treated *P. kessleri* cells was performed with two biological replicates (R1 and R2). In total, 93 proteins were identified in R1 and 152 were identified in R2 (Supplemental Table S2). Of these proteins, 31 that are potentially involved in the roles of LDs are listed in Table 3. Among these proteins, 13 were of plastidial origin. Goold et al. (2016) also detected a large portion of plastidial proteins in LDs, but they could not tell if these proteins were contamination resulting from sample preparation. In our opinion, these plastidial proteins are integral parts of the LD proteome, as we found red chlorophyll fluorescence present in LDs using confocal microscopy (Fig. 3, O, P, R, and S). Moreover, the extracted LDs and LDs from ruptured cells (created by pressing the cover slip with a finger, resulting in rupture of the salt-treated cells) contained chlorophyll (Supplemental Fig. S6). These results suggest that chloroplast components are converted to LDs.

Proteins associated with lipid synthesis in this study include acetyl-CoA carboxylase and 1-acyl-*sn*-glycerol-3-phosphate acyltransferase identified in R1; 3-ketoacyl-CoA synthase and long-chain acyl-CoA synthetase identified in R2; and diacylglycerol kinase identified in both replicates. The presence of these proteins supports the idea that LDs are involved in the synthesis of membrane PLs. The additional proteins identified in LDs included mitochondrial proteins, endoplasmic reticulum-related proteins, heat shock

Table 3. *Description of putative proteins in salt-induced LD proteomics of* P. kessleri

P, Present; R1, occurrence in replicate 1; R2, occurrence in replicate 2; –, not detected.

No.	Mascot Protein Score	Protein Description	R1	R2
1	496	ATP synthase subunit α	P	P
2	519	ATP synthase subunit β	P	P
3	551	PSII protein D1	P	P
4	741	Chlorophyll *a*/*b*-binding protein	P	P
5	1,090	PSII CP43 reaction center protein	P	P
6	296	Rubisco activase	P	P
7	875	PSII CP47 reaction center protein	P	P
8	50	30S ribosomal protein S4	P	P
9	227	Starch synthase	P	P
10	381	PSI P700 chlorophyll *a* apoprotein A2	P	P
11	702	PSII D2 protein	P	P
12	50	ATP synthase subunit b	P	P
13	125	Oxygen-evolving enhancer protein (fragment)	P	P
14	46	Cytochrome *c1-1*, heme protein	P	P
15	39	Succinate dehydrogenase (ubiquinone) iron-sulfur subunit	P	P
16	195	Putative mitochondrial-processing peptidase subunit α-1	P	P
17	122	NAD(P) transhydrogenase, mitochondrial	P	P
18	1,401	ADP, ATP carrier protein	P	P
19	69	Cytochrome *c* oxidase subunit 2	P	P
20	205	Cytochrome *f*	P	P
21	56	Glyceraldehyde 3-phosphate dehydrogenase	P	P
22	62	Calreticulin 2, calcium-binding protein	–	P
23	85	ADP-ribosylation factor	P	P
24	54	Ras-related protein Rab7	P	P
25	46	Diacylglycerol kinase	P	P
26	387	Heat shock protein70	P	P
27	46	Histone H2B	P	P
28	62	Acetyl-CoA carboxylase	P	–
29	53	1-Acyl-*sn*-glycerol-3-phosphate acyltransferase	P	–
30	55	3-Ketoacyl-CoA synthase	–	P
31	45	Long-chain acyl-CoA synthetase	–	P

protein70, histone H2B, and vesicle trafficking and transport proteins (ADP-ribosylation factor and Ras-related protein Rab7), suggesting that LDs are highly dynamic and complex.

Ultrastructure Studies of Cells by Transmission Electron Microscopy

Histones stored on LDs are suggested to facilitate rapid chromatin assembly during early embryonic development in *Drosophila melanogaster* (hereafter *Drosophila*; Li et al., 2012b). Histone H2B is present in salt-induced LDs, which led us to question the functions of LDs. To test whether histones help store material for future use when cells are coping with salt stress, we carried out a stress repair experiment. In this experiment, cells were cultivated in the presence of 350 mM NaCl for 12 d, after which they were collected and resuspended in fresh 100 mM NaCl-containing medium for 1 d. Then, the stress repair cells, together with salt-treated and untreated cells, were analyzed by transmission electron microscopy (TEM).

TEM analysis showed that LDs were absent in untreated *P. kessleri* cells (Fig. 5A), whereas many LDs of 0.2 to 0.7 μm diameter were distributed around the plasma membrane in salt-treated cells (Fig. 5, B–F), in line with the confocal microscopy observations (Fig. 3, I, L, O, and R). These LDs were bigger in smaller cells than in larger cells, implying that LDs shrank as the plasma membrane expanded (Fig. 5B; Supplemental Fig. S7). In addition, LDs seemingly located inside the plastid (Fig. 5C, arrowhead) where the chloroplast degraded (Fig. 5B), which further confirmed the possible translocation of components from chloroplast to LDs. In the stress repair conditions where the cells resumed division, within just 24 h LDs increased in size (0.3–2.5 μm) and the chloroplast was restored (Fig. 5, G–I). These results suggest that LDs may contribute to cell division and chloroplast reconstruction, likely by providing histones and chloroplast components for rapid chromatin and chloroplast assembly.

Besides LDs, another unique feature of salt-treated cells was the occurrence of autophagy vacuoles (Fig. 5B). These autophagy vacuoles were associated with LDs. For example, some LDs were partially extruded into the autophagy vacuole (Fig. 5, D and E, arrowheads) and other LDs were completely engulfed by the autophagy vacuole (Fig. 5F, arrowhead). Autophagy vacuoles decreased both in size and abundance in stress repair cells (Fig. 5, G–I) compared with those in salt-stressed cells (Fig. 5B).

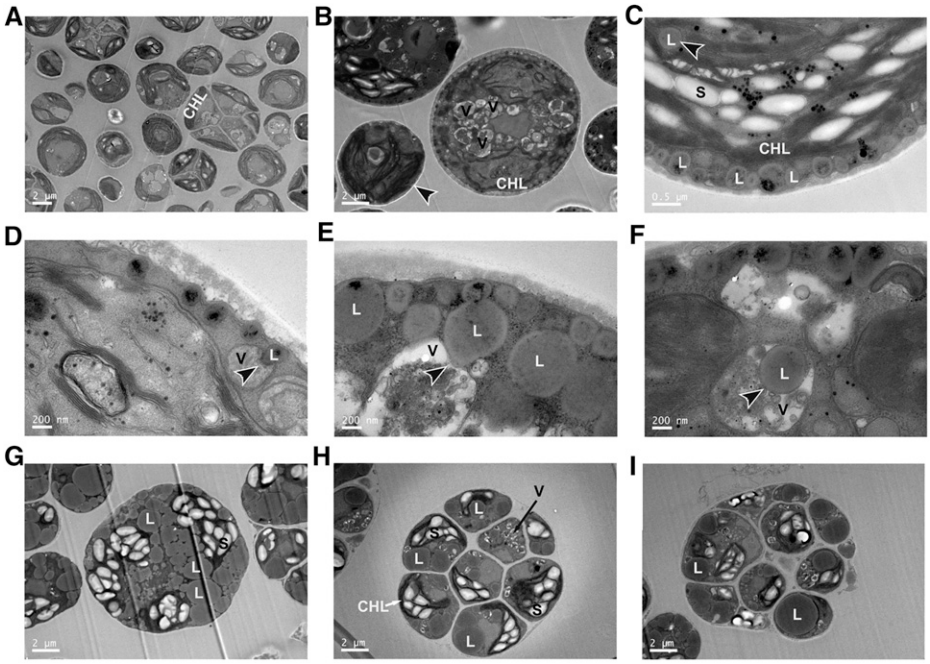

Figure 5. TEM images of *P. kessleri* cells during salt stress and stress repair. A, *P. kessleri* cells cultivated under control conditions. B to F, *P. kessleri* cells cultivated under salt stress. G to I, Changes of stress repair in *P. kessleri* cells (after treatment with 350 mM NaCl for 12 d, *P. kessleri* cells were transferred into fresh 100 mM NaCl-containing TAP medium for 1 d). CHL, Chloroplast; L, lipid droplet; S, starch granule; V, vacuole. The black arrowhead in B indicates a salt-treated cell that did not contain LDs and autophagy vacuoles. The black arrowheads in C to F indicate LDs. The black and white arrows in H indicate vacuole and chloroplast, respectively.

LD Population Distribution and Growth

We also found a group of salt-treated cells that did not contain LDs and autophagy vacuoles, similar to untreated cells (Fig 5B, arrowhead), which indicated that LD accumulation differed among salt-treated cells. Thus, Nile Red was used for analysis of LD population distribution by flow cytometry. Salt-treated cells showed a higher value both in forward scatter and side scatter, implying increases in cell size and granularity compared with untreated cells. This was consistent with our confocal microscopy (Fig. 3) and TEM (Fig. 5, A and B) observations. Moreover, salt-treated cells displayed two fluorescence peaks (Fig. 6A), suggesting that salt stress induced the cells into an LD-high subpopulation and an LD-free or LD-low subpopulation. Upon steady-state salt exposure, large cells accumulated LDs whereas small cells tended not to (Fig. 6A). The growth and division of neural stem cells correlates with hypoxia-induced LDs in neighboring glial cells in *Drosophila* (Bailey et al., 2015). As shown in Figure 6B, cell growth showed a 9-fold increase after 12 d of cultivation under salt stress, which implies that LDs may play a positive role in cell growth under salt stress.

To test whether salt-induced LDs have a beneficial role in the growth of *P. kessleri*, we used acetate to change the LD content, which allowed us to investigate the effect of LDs on growth despite the lack of LD mutants. Acetate can stimulate LD production (Goodson et al., 2011), and ^{13}C-labeled acetate was incorporated into the core of hypoxic LDs in *Drosophila* (Bailey et al., 2015). We cultivated *P. kessleri* cells under 350 mM NaCl conditions with or without acetate addition and examined culture OD_{640} and LD content by Nile Red staining. As shown in Figure 6, E and F, the mean forward scatter and PE of *P. kessleri* cells under acetate conditions was approximately 1.3- and 10-fold as high, respectively, as that without acetate conditions, indicating increases both in cell size and LD content with acetate. *P. kessleri* cultures with acetate containing high LD showed a 3-fold increase in OD_{640} as compared with cultures without acetate containing low LD (Fig. 6, C and D). These results further confirm that LD content is positively correlated with the increase in cell size and the growth of cultures.

DISCUSSION

In this study, we showed that salt stress is associated with increased cell size and LD content in *P. kessleri*. Transcriptomic analysis revealed that salt stress upregulated genes associated with compatible solute synthesis (Pro) and antioxidant enzymes (CAT); however, genes associated with the Lands cycle were also overexpressed. We further showed that some LDs were located along the plasma membrane, and enzymes related to the synthesis of membrane PLs were identified in LDs. These data suggest that, in addition to osmotic regulation and antioxidant systems, LDs might also have a crucial function in the response to salinity stress.

LDs Participate in Defense against Salt Stress by Providing Materials and Enzymes for Membrane Reconstruction

LDs were historically overlooked as passive lipid storage compartments but are now considered central, active players in lipid homeostasis (Welte, 2007). Approximately 160 PL molecular species have been identified in isolated LDs, with an enrichment in

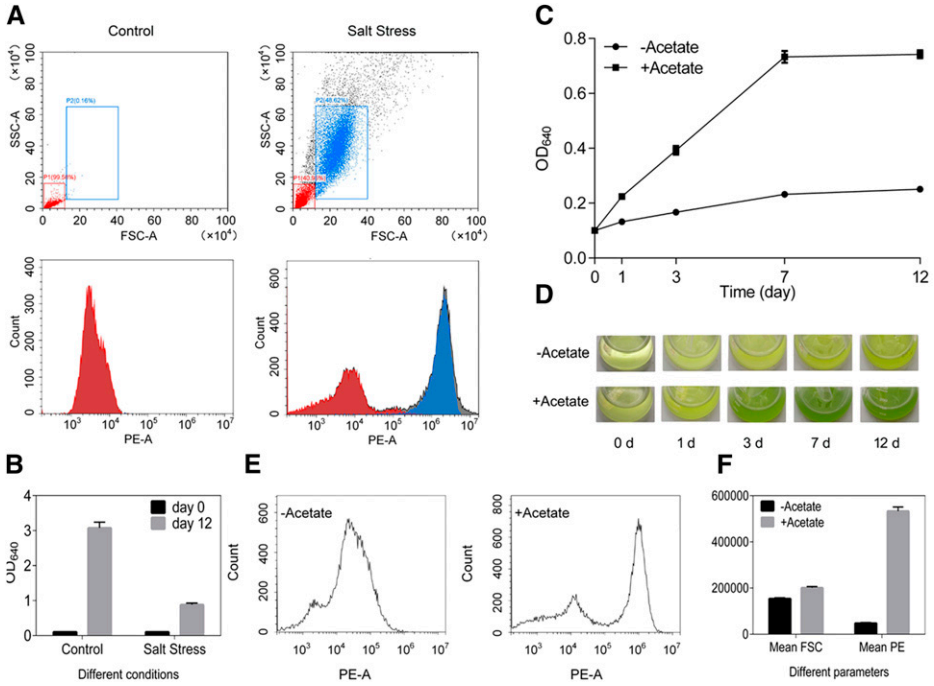

Figure 6. LD population distribution of *P. kessleri* cells and relationship between LD content and growth. A, Flow cytometry analysis of Nile Red-stained *P. kessleri* cells cultivated under control and salt-stress conditions for 12 d. FSC-A and SSC-A represent forward-scattered and side-scattered light signals, respectively. PE-A represents Nile Red fluorescence signal. The P1 subpopulation appears red and the P2 subpopulation appears blue. Gray represents cells out of the P1 and P2 subpopulations. B, Growth of *P. kessleri* cells over a 12-d period of cultivation under different experimental conditions. C, Growth of *P. kessleri* cells cultivated under salt-stress conditions (350 mM NaCl) with (+Acetate) or without (−Acetate) acetate addition for 1, 3, 7, and 12 d. D, Visual observation of *P. kessleri* cells cultivated under 350 mM NaCl conditions with or without acetate addition at different time points. E, Analysis of LDs in Nile Red-stained *P. kessleri* cells cultivated under salt-stress conditions with or without acetate addition by flow cytometry. F, FlowJo analysis of cell size and LD content through the values of FSC-A and PE-A. Values are means ± SD of three independent biological replicates in B, C, and F.

lysophospholipids, further indicating that LDs function in PL traffic (Bartz et al., 2007). The presence of long-chain acyl-CoA synthetase3 and LPCAT in LDs suggested that LDs could generate phosphatidylcholine from lysophosphatidylcholine in situ, thus contributing to membrane expansion (Massey et al., 1997; Moessinger et al., 2014; Barneda and Christian, 2017). In this study, genes encoding LPLATs were significantly up-regulated by salt stress (Fig. 2). As a result, 1-acyl-*sn*-glycerol-3-phosphate acyltransferase was found in salt-induced LDs (Table 3). These LDs also contained long-chain acyl-CoA synthetase and diacylglycerol kinase (Table 3), implying that LDs could likely produce PLs in situ. Moreover, salt-induced LDs were located close to the plasma membrane (Figs. 3, I, L, O, and R, and 5, B–F), with larger LDs abundant in smaller cells and smaller LDs present in larger cells (Fig. 5B; Supplemental Fig. S7). These features suggest that LDs provide substances for PL production, which contributes to plasma membrane expansion while causing a reduction in LD volume (Fig. 7).

In addition, genes encoding PLA2s were also overexpressed (Table 1), which meant enhanced hydrolysis at the *sn*-2 position of PLs and overproduction of lysophospholipid. These lysophospholipids could also contribute to PL production. Intact cells of *P. kessleri* produced mainly C18:2 and C18:3, with undetectable C18:1 under control conditions; however, salt-treated cells contained a reduced proportion of C18:3 and increased proportions of C18:1 and C18:2 (Fig. 4, A and B; Table 2). Enhanced hydrolysis at the *sn*-2 position of PLs may be associated with the altered FA composition following exposure to salt. Phospholipids acquire their appropriate FA composition through the Lands cycle (Lands, 1958). In the Lands cycle, PLA2 hydrolyzes inappropriate fatty acyl chains at the *sn*-2 position of PLs to form lysophospholipid, which is then reacylated together with appropriate fatty acyl chains by LPLATs to produce new PLs (Lands, 2000; Shimizu et al., 2006).

The FA composition of membrane lipids affects biological processes such as lipid packing and membrane fluidity (Graef, 2018). A decrease in unsaturated FAs and a subsequent decrease in membrane fluidity could contribute to salt tolerance (Mansour et al., 2015). In addition, unsaturated FAs increase susceptibility to oxidative attack (Bailey et al., 2015; Mansour et al., 2015). In yeast cells, overexpression of Δ-12 desaturases resulted in increased tolerance to high salt (Rodríguez-Vargas et al., 2007).

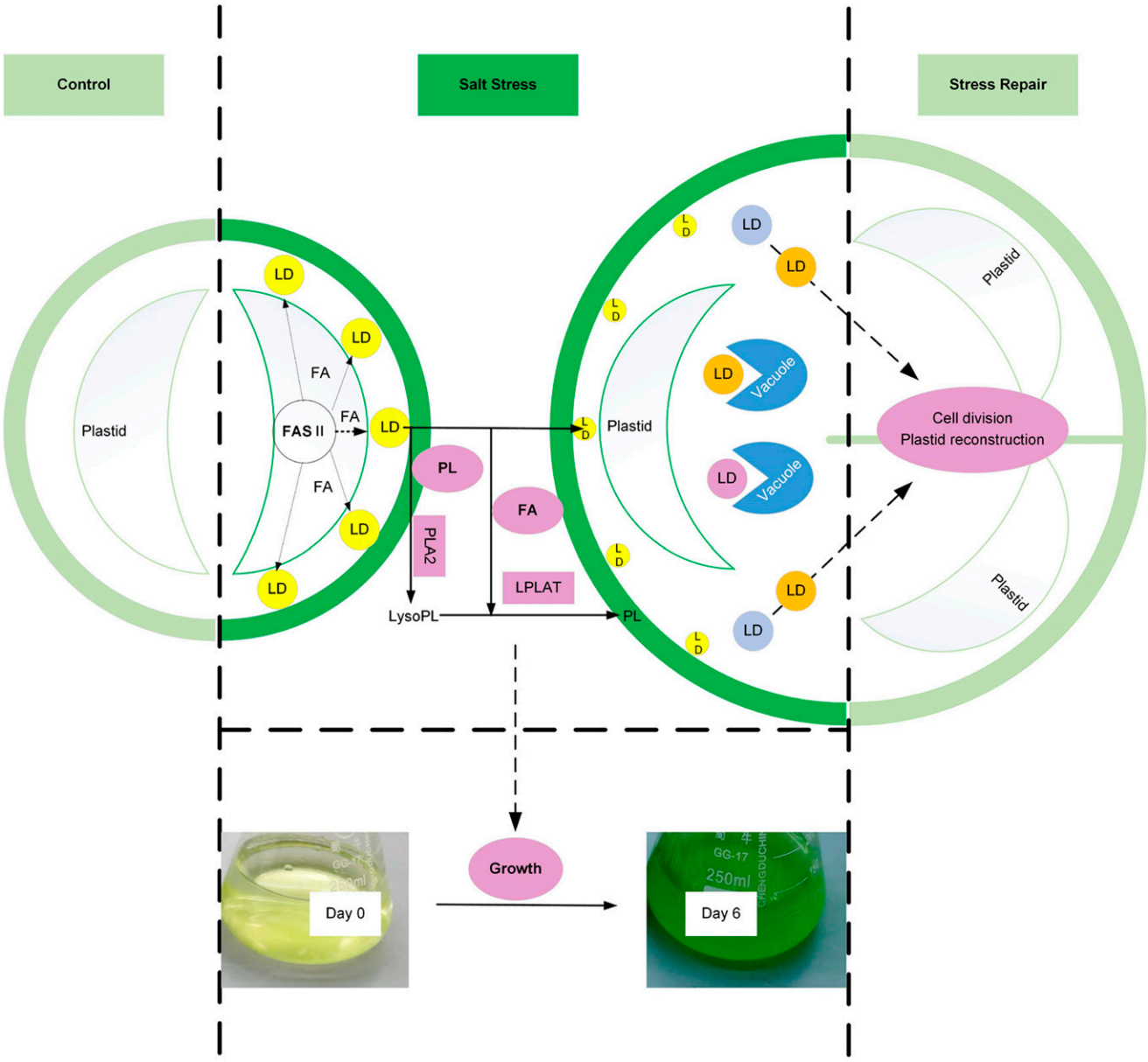

Figure 7. Proposed roles of LDs in *P. kessleri* cells in response to salt stress. The light or dark green membranes imply variations of FA composition or surface of membrane. Different colors of LDs suggest diverse roles (yellow LDs are involved in membrane remodeling, orange LDs contain chlorophyll, purple LDs are related to cytoplasmic component recycling, and blue LDs harbor proteins for future use). The day 0 image depicts cells that were just transferred into 350 mM NaCl-containing TAP medium. The day 6 image depicts cells that were incubated in 350 mM NaCl-containing medium for 6 d. FAS II, Fatty acid synthesis pathway.

To reduce membrane susceptibility to oxidative attack and concomitantly maintain appropriate membrane fluidity, salt-treated cells overexpressed desaturases, accumulating C18:1 and C18:2 and reducing C18:3 (Fig. 4, A and B; Table 2), and accomplished membrane remodeling with the help of PLA2s and LPLATs. The reduced C18:3 in PL (Fig. 4, A and B), the presence of a small amount of C18:3 and proteins associated with lipid synthesis in LDs (Tables 2 and 3), and the transfer of fluorescent FA from membrane lipids to LDs (TAG; Fig. 4C) suggested that this membrane remodeling was associated with LDs. The enrichment of C18:1 and C18:2 in LDs and shrunken LDs suggested that LDs harbored unsaturated FAs and supplied substances for membrane remodeling. Taken together, these data imply that, under salt stress, LDs participated in reconstruction of membrane PLs, including membrane modification and plasma membrane expansion (Fig. 7).

LDs Play a Role in Cytoplasmic Component Recycling during Salt Stress

We searched for homologs of major lipid droplet protein, a major structural protein of *Chlamydomonas* LDs (Moellering and Benning, 2010), in *P. kessleri*. We also checked for homologs to other dominant LD structural proteins like lipid droplet surface protein in *Nannochloropsis oceanica* and oleosin in plants. However, we did not identify these homologs. It is unclear if *P. kessleri* LDs lack structural proteins, as has been observed in yeast LDs (Huang, 2018). We also did not observe the lipases involved in LD breakdown by lipolysis. Whereas LD-resident lipases play a central role, LDs can also be mobilized through macroautophagy, which is termed lipophagy. Macroautophagy-mediated LD degradation is associated with GTPase Rab7, a strong candidate for selection of LDs as lipophagic substrates (Lizaso et al., 2013; Schroeder et al., 2015). Ras-related protein Rab7 was identified in salt-induced LDs (Table 3), and a single LD was completely engulfed by a vacuole (Fig. 5F), indicating that lipophagy occurred in salt-treated cells. Lipophagy can also power the biogenesis of LDs by releasing FAs that can be reesterified and stored as neutral lipids (Rambold et al., 2015). Under salt stress, lipophagy may be involved in recycling cellular building blocks such as FAs to ensure LD homeostasis.

Autophagy is involved in chloroplast degradation in Arabidopsis (*Arabidopsis thaliana*; Wada et al., 2009). Furthermore, Rubisco, the most abundant chloroplast protein, can be transported into Rubisco-containing bodies for subsequent degradation by autophagy (Ishida et al., 2008; Wada et al., 2009). In this study, chloroplast components were converted into LDs, LDs were found in vacuoles, and the chlorophyll concentration decreased (Fig. 1C). However, whether there is an LD-mediated chloroplast degradation pathway in salt-stressed cells is unknown. Some LD-bound proteins are destined for degradation, whereas others are released and reused (Welte, 2007). It remains unknown how this protein selection is regulated. The reduction of vacuoles in stress repair cells implied a transition from rough degradation to fine degradation. Rough degradation by vacuoles under salt stress emphasizes substance recycling, whereas fine degradation might be associated with material reuse due to reexamination. These hypotheses should be tested in future studies.

LDs Harbor Proteins from Other Cellular Compartments during Salt Stress

Previous studies revealed that *Chlamydomonas* employs a chloroplast pathway for TAG biosynthesis and formed LDs inside the chloroplast (Fan et al., 2011). In *Chlamydomonas* and *Klebsormidium nitens*, the formation of large LDs is accompanied by chloroplast degradation, indicating that chloroplast materials are converted into LDs (Kuroiwa et al., 2014). We found a single LD seemingly inside the chloroplast in salt-treated cells (Fig. 5C). We also found chlorophyll fluorescence (Fig. 3, P and S) and proteins of plastidial origin (Table 3) in salt-induced LDs. These results suggest that chloroplast components are transported to LDs under salt stress, similar to what occurs in starved cells.

In addition to plastidial proteins, histone H2B was also identified in salt-induced LDs (Table 3). LD-bound histones are found in *Drosophila* embryos, and the protein Jabba has been identified as the histone anchor on LDs. Ongoing research suggests that LDs store proteins and LD-bound histones support rapid chromatin assembly during early embryonic development (Cermelli et al., 2006; Li et al., 2012b; Welte and Gould, 2017). In stress repair cells, the enlarged LD size and reduced LD numbers suggested that LDs fuse to form large LDs, as shown in Figure 5E. This fusion will reduce LD surface/volume ratio and result in a surplus of membrane components. What is the fate of the spare membrane components? In plant oilseeds, stored oils are mobilized to produce sugars that are important for germination and seedling establishment (Eastmond, 2006; Graham, 2008). In *Chlamydomonas*, the disappearance of accumulated LDs is accompanied by the resyntheses of photosynthetic membranes and regain of vegetative growth (Siaut et al., 2011). In this study, the resumed division of mother cells and restored chloroplasts in each daughter cell after destress (Fig. 5H) were also found. This phenomenon led to the hypothesis that LD fusion was accompanied by unloading of membrane components such as plastidial proteins and histone H2B, which might contribute to rapid construction of organelles, for example chromatin and chloroplasts (Fig. 7).

LDs May Contribute to *P. kessleri* Growth during Salt Stress

The *Chlamydomonas pgd1* mutant, defective in TAG accumulation, exhibits a loss of viability under nitrogen deprivation (Li et al., 2012a). The growth of *P. kessleri* under salt stress is positively correlated with LD content (Fig. 6, C–E), suggesting that LDs play a beneficial role in salt-stress tolerance. In addition, salt-treated cultures were divided into two subpopulations. One comprised LD-free small cells and the other had LD-high large cells (Fig. 6A). In *Drosophila*, the capability of neural stem cells to grow and divide is associated with the induction of LDs in neighboring glial cells during hypoxia (Bailey et al., 2015). The phenomenon that a subpopulation of cells accumulate LDs and lead to protection of the entire tissue is also present in the mouse liver (Herms et al., 2013). In this study, salt-treated cultures showed an increase in growth, indicating that cell division did not cease (Fig. 6B). LD-high cells contained autophagy vacuoles and degraded chloroplasts and, under the stress repair conditions, these cells resumed division (Fig. 5, B and G–I), implying that LD-high cells lost the ability to divide

during salt stress. These data suggest that salt stress might result in functional differentiation: some cells are responsible for division, others for the accumulation of LDs. Fat-specialized cells can be found from flies to humans, hinting that fat compartmentalization may be an evolutionarily positive trait. Herms et al. (2013) further demonstrated that LD-high cells lead to protection of the entire tissue by providing stored lipids to LD-low cells. In this study, LD-high cells under salt stress might also provide material support for LD-free small cells and thus contribute to cell growth and a reduced rate of cell death, comparable to what occurs in the mouse liver (Herms et al., 2013).

CONCLUSION

In this study, we provide evidence that LDs serve as a mobile rescue station, a role that involves membrane reconstruction, protein storage, and cytoplasmic components recycling in response to salt stress. In addition, high-LD cells might be crucial for the survival and reproduction of the whole population. Our data suggest that LDs are used as a protective mechanism to help cells survive under salt stress and also to lay a material foundation for growth. The level of LD content can serve as an indicator of cell state, since the more of the rescue stations there are, the more precarious the cell survival likelihood is.

MATERIALS AND METHODS

Microalgal Strain and Growth Conditions

The microalga used in this study was provided by Ghopur Mijit. This strain was identified as *Parachlorella kessleri*. Cells were maintained in 250-mL flasks containing 150 mL of TAP medium (Harris, 2001) at 25°C ± 1°C with shaking at 100 rpm under constant illumination (100 μmol photons m^{-2} s^{-1}). For salt-stress conditions, *P. kessleri* cells were grown in TAP medium until they reached the exponential phase of growth (optical density (OD) between 0.7 and 1 at $\lambda = 640$ nm), and then cells were spun at 5,000 rpm for 5 min at 25°C (rotor, F-34-6-38) followed by resuspension in TAP medium without salt or with 350 mM NaCl (OD ~ 0.1). For synchronization, cells were in Erlenmeyer flasks in inorganic high-salt medium, alternating 14-h/10-h light/dark cycles, at 100 μmol photons m^{-2} s^{-1} at 25°C ± 1°C (Bisova et al., 2005). For the stress repair experiment, cells were cultivated under 350 mM NaCl for 12 d, after which they were collected and resuspended in fresh 100 mM NaCl-containing TAP medium for 1 d. The cell volume was measured with a Beckman Z2 (Beckman Coulter).

Quantification of Cell Biochemical Composition

To determine carbohydrate content, freeze-dried algae power (0.1 g) was suspended in 2 mL of 6 M HCl and 3 mL of distilled water and boiled for 30 min until the carbohydrate was hydrolyzed into Glc. Then the samples were analyzed using the phenol-sulfuric acid method (Dubois et al., 1956).

Protein content of *P. kessleri* cells was determined using the colorimetric method (Bradford, 1976). Freeze-dried algae power (0.02 g) was suspended in 1 mL of buffer containing 2% (w/v) SDS, 10% (v/v) glycerol, 50 mM Tris-HCl (pH 8), and 1 mM DDT. After homogenization, the samples were centrifuged at 12,000 rpm (rotor, F-45-30-11) for 20 min. The supernatant fraction was used for the determination of protein content.

Total lipids were extracted from *P. kessleri* cells with a modified protocol of Zhu et al. (2002). Freeze-dried algae power (0.1 g) was suspended in a 1-mL solvent mixture of chloroform:methanol (2:1, v/v). After homogenizing for 10 min, the samples were centrifuged at 10,000 rpm for 10 min. The procedure was repeated four times until total lipids were fully extracted. Then the solvent phase from each replicate was transferred and evaporated at 60°C. The total lipids were weighed using an analytical balance (BS 124S; Sartorius).

TAGs were quantified using a densitometry method by comparison with a standard curve generated from known amounts of glycerol trioleate standard. Total lipids (20 μg) were loaded as a spot onto 10- × 20-cm silica gel HSGF254 HPTLC plates (Yantai Jiangyou). Plates were developed using double development (two-thirds in acetone:toluene:water [91:30:8, v/v/v] followed by full development in hexane:diethyl ether:acetic acid [70:30:1, v/v/v]; Fan et al., 2011). After plates were thoroughly dried, they were dipped for 6 s in a $CuSO_4$ reagent (Churchward et al., 2008; 20 g of $CuSO_4$, 200 mL of methanol, 8 mL of H_2SO_4, and 8 mL of H_3PO_4), heated at 141°C for 30 min in an oven, and finally scanned using Gel DocTM XR+ (Bio-Rad).

RNA Extraction, Sequencing, Data Analysis, and Validation

Total RNA from three independent cultures was isolated using TRIzol Reagent (Invitrogen) and purified with Plant RNA Purification Reagent (Invitrogen). RNA quality was determined using an Agilent 2100 BioAnalyzer. RNA sequencing and data analysis were done by Majorbio (Shanghai Majorbio Bio-Pharm Technology).

The differential expression of genes involved in pathway reconstruction is listed in Supplemental Table S3. To confirm RNA sequencing results, the expression levels of several genes under control and salt-stress conditions were measured using RT-qPCR. The cDNA was synthesized using reverse transcriptase according to the manufacturer's instructions (TaKaRa Biotech). Primers used are listed in Supplemental Table S1. qPCR was performed with the CFX96 Touch Real-Time PCR Detection System (Bio-Rad) using SYBR Green (Tiangen Biotech). The real-time PCR cycle was 95°C for 15 min followed by 40 cycles at 95°C for 10 s and 60°C for 30 s. Triplicate qPCRs were performed for each sample. G-protein β-subunit-like polypeptide was used as an internal reference to normalize the expression data. The ΔΔCT method was applied to measure the target gene expression.

Pulse-Chase Experiments

Pulse-chase labeling of lipids in *P. kessleri* was performed using Bodipy FL C12 (Invitrogen, Life Technology). Cells were incubated with Bodipy FA for 3 d and then harvested and washed three times. Then they were suspended in unlabeled fresh TAP medium with/without salt for 1, 3, or 7 d. The 488-nm laser line was used to image Bodipy FL C12 using confocal microscopy. Signals were collected between 500 and 530 nm. Labeled lipids in cells were extracted, lipid classes were resolved on TLC plates, and the plates were scanned using Gel DocTM XR+ (Bio-Rad).

Microscopy

To assess the morphological changes such as difference in cell size, microscopic analysis of cells was done with an Olympus CX41 microscope and a confocal microscope (TCS SP8 STED 3X; Leica). To investigate LD distribution, samples were stained first with Nile Red following the manufacturer's protocols (GenMed Scientifics; GMS80050.1) and then imaged with a confocal microscope using an oil-immersion objective. The Nile Red signal was captured using a laser excitation line at 488 nm, and emissions were captured at 539 to 591 nm. Chlorophyll autofluorescence was collected at 620 to 700 nm. For TEM, *P. kessleri* cells were fixed overnight in 2.5% (v/v) glutaraldehyde (pH 7.4) at 4°C. Samples were pretreated using conventional protocols, including dehydration, mixing, embedding, and sectioning (Roomans, 1999). Cells were imaged using a transmission electron microscope (Tecnai G2 spirit Biotwin).

Isolation of LDs

The LD isolation protocol established in *Chlamydomonas reinhardtii* (hereafter *Chlamydomonas*) was used to isolate salt-induced LDs (Goold et al., 2016). Briefly, cells were harvested by centrifugation and then suspended in HEPES-KOH buffer (25 mM, pH 7.5) containing 0.6 M Suc and a protease inhibitor cocktail for plant cells (Sangon Biotech). To break the cells, the cell suspension was homogenized using glass beads (Sigma; 425–600 μm). After washing with

Tween, NaCl, urea, and Suc-free buffer, the LDs on top were collected and stored at −80°C for further analysis.

Protein Extraction, SDS-PAGE, and Proteomic Analysis

Proteins were extracted from isolated LDs by adding cold acetone (80%, v/v). Extracted proteins were separated by SDS-PAGE according to standard protocols. Proteins were then stained with Coomassie Brilliant Blue. Bands were cut and submitted to nano-liquid chromatography analysis (UltiMate3000 RSLCnano liquid chromatograph). The protein database used for Mascot (version 2.4.1; Matrix Science) searches included Chlorophyta downloaded from UniProt (a total of 48,736 entries).

FA Analysis

The FA methyl ester compositions of algal cells and LDs under control and salt-stress conditions were analyzed after the acidic transesterification of lipids (Miao et al., 2009). Extracted lipids were first combined with 5 mL of H_2SO_4 (5%, v/v) and then reacted at 80°C for 2 h in a water bath. After cooling, 1 mL of hexane and 1 mL of water were added to samples, which were then stirred gently and centrifuged. One microliter of the organic upper phase, which contained the FA methyl esters, was injected into an Auto System XL GC/Turbo Mass MS (PerkinElmer) using a DB-5MS (5% phenyl)-methylpolysiloxane nonpolar column (30 m × 0.25 mm × 0.25 μm; Tang et al., 2011).

Flow Cytometry Analysis

Cell samples (about 10^6 cells mL^{-1}) were collected and stained using Nile Red according to the manufacturer's protocols (GenMed Scientifics; GMS80050.1). After incubating for 10 min at room temperature in darkness, samples were analyzed using a Cytoflex (Beckman Coulter) equipped with a 488-nm laser.

To detect the percentage of dead cells, we used SYTOX Green (Invitrogen, Life Technology), a high-affinity nucleic acid stain that easily penetrates those cells with compromised cell membranes but not those with healthy cell membranes. Cell samples (about 10^6 cells mL^{-1}) were incubated with SYTOX Green (final concentration in 1 mL of culture is 5 μM) for 20 min at room temperature. Samples were analyzed without washing or fixing using Cytoflex with 488 nm excitation and emission collected in a 525/30 bandpass filter or equivalent.

We measured total ROS with the membrane-permeant fluorescence indicator 2′,7′-dichlorodihydrofluorescein diacetate (H2DCFDA; Invitrogen, Life Technology) using the modified method of Hakkila et al. (2014). Cell samples (about 10^6 cells mL^{-1}) were incubated with H2DCFDA (final concentration in 1 mL of culture is 10 μM) for 90 min in complete darkness at 32°C. Cells were washed with TAP medium and suspended with TAP medium. Fluorescence from H2DCFDA was measured using Cytoflex with 488 nm excitation and emission collected in a 525/30 bandpass filter or equivalent.

Lipid Analysis by UHPLC

Total lipid separation was carried out using an ACQUITY UPLC BEH C18 analytical column (100 × 2.1 mm, 1.7 μm; Waters) using the modified method described by Su et al. (2017). Mobile phases were acetonitrile:water (60:40, v/v) with 10 mM ammonium formate and 0.1% (v/v) formic acid (A) and isopropanol:acetonitrile (90:10, v/v) with 10 mM ammonium formate and 0.1% (v/v) formic acid (B). The following gradient was performed at a flow rate of 0.4 mL min^{-1}: 0 to 0.5 min, 95% A; 2 to 2.1 min, 57% A; 12 min, 50% A; 12.1 min, 46% A; 18 min, 30% A; and 18.1 to 20 min, 95% A. The injection volume was set to 1 μL, and the column temperature was set to 55°C.

Mass spectrometry was performed on a Thermo Scientific Q Exactive hybrid quadrupole-Orbitrap mass spectrometer with electrospray ionization source according to the modified method described by Criscuolo et al. (2019). Spray voltage was set at 3.2 kV in positive and 2.8 kV in negative ion mode. The capillary temperature, auxiliary gas heater temperature, sheath gas flow, auxiliary gas flow, and s-lens Radio Frequency level were set at 320°C, 350°C, 50 arbitrary units, 15 arbitrary units, and 50 V, respectively. The values of the maximum injection time and automatic gain control were 100 ms and 1e6. For full mass acquisition, data were collected in the range 150 to 2,000 atomic mass units with 70,000 resolution. For data-dependent tandem mass spectrometry acquisition, spectral information was acquired with a resolution of 17,500, automatic gain control of 5e5, and injection time of 50 ms. Nitrogen (99.999%) was used as collision-induced dissociation gas. The collision energy was set at 15, 30, and 45 kV.

The data were obtained in raw files with the XCalibur software (Thermo Fisher Scientific). The identification, alignment, and quantification were finished through lipidsearch 4.1 (Thermo Fisher Scientific). Then the corrected peak areas of all identified lipid species were used for further analysis.

Statistical Analysis

For two-group comparison, Student's t test was performed to determine statistically significant differences. $P < 0.05$ was considered statistically significant. Data are means ± SD of three independent biological replicates.

Accession Numbers

Sequence data from this article can be found in the GenBank/EMBL data libraries under accession number GSE134786.

Supplemental Data

The following supplemental materials are available.

Supplemental Figure S1. Synchronization analysis and DIC images of *P. kessleri* in response to salt stress.

Supplemental Figure S2. Validation of relative expression levels of selected genes by RT-qPCR.

Supplemental Figure S3. Determination of TAG content in response to salt stress using TLC.

Supplemental Figure S4. Localization of Bodipy FL C12 in *P. kessleri* under salt stress.

Supplemental Figure S5. Pulse-chase labeling of lipids in *P. kessleri* using Bodipy FL C12.

Supplemental Figure S6. Images of the extracted LDs and LDs from ruptured cells.

Supplemental Figure S7. Size changes of LDs present along the plasma membrane in *P. kessleri* cells treated with 350 mM NaCl.

Supplemental Table S1. Primers used in this study for RT-qPCR analysis.

Supplemental Table S2. Proteomic analyses of LDs isolated from salt-treated *P. kessleri* cells.

Supplemental Table S3. Differential expression of genes involved in the pathway reconstruction in Figure 2.

ACKNOWLEDGMENTS

We thank Ghopur Mijit (Xinjiang University) for providing microalgal strains as well as Dr. Feng Lei, Di Ling, Gao Mei, Wang Ge, Hou Jingli, and Yuan Jiaojian (Instrumental Analysis Center of Shanghai Jiao Tong University) for their excellent technical help.

Received June 3, 2019; accepted July 11, 2019; published July 24, 2019.

LITERATURE CITED

Andreas K, Dietmar F, Ina P, Uwe J, Gerhard D (2007) Regulation of proline metabolism under salt stress in the psychrophilic diatom *Fragilariopsis cylindrus* (Bacillariophyceae). J Phycol **43:** 753–762

Avidan O, Pick U (2015) Acetyl-CoA synthetase is activated as part of the PDH-bypass in the oleaginous green alga *Chlorella desiccata*. J Exp Bot **66:** 7287–7298

Bailey AP, Koster G, Guillermier C, Hirst EM, MacRae JI, Lechene CP, Postle AD, Gould AP (2015) Antioxidant role for lipid droplets in a stem cell niche of *Drosophila*. Cell **163:** 340–353

Barneda D, Christian M (2017) Lipid droplet growth: Regulation of a dynamic organelle. Curr Opin Cell Biol **47:** 9–15

Bartz R, Li WH, Venables B, Zehmer JK, Roth MR, Welti R, Anderson RGW, Liu P, Chapman KD (2007) Lipidomics reveals that adiposomes store ether lipids and mediate phospholipid traffic. J Lipid Res **48:** 837–847

Bisova K, Krylov DM, Umen JG (2005) Genome-wide annotation and expression profiling of cell cycle regulatory genes in *Chlamydomonas reinhardtii*. Plant Physiol **137:** 475–491

Blazeck J, Hill A, Liu L, Knight R, Miller J, Pan A, Otoupal P, Alper HS (2014) Harnessing *Yarrowia lipolytica* lipogenesis to create a platform for lipid and biofuel production. Nat Commun **5:** 3131

Borowitzka MA, Moheimani NR (2013) Sustainable biofuels from algae. Mitig Adapt Strategies Glob Change **18:** 13–25

Borowitzka MA, Beardall J, Raven JA (2016) The Physiology of Microalgae. Springer International Publishing, Developments in Applied Phycology

Bradford MM (1976) A rapid and sensitive method for the quantitation of microgram quantities of protein utilizing the principle of protein-dye binding. Anal Biochem **72:** 248–254

Bromke MA, Giavalisco P, Willmitzer L, Hesse H (2013) Metabolic analysis of adaptation to short-term changes in culture conditions of the marine diatom *Thalassiosira pseudonana*. PLoS ONE **8:** e67340

Cermelli S, Guo Y, Gross SP, Welte MA (2006) The lipid-droplet proteome reveals that droplets are a protein-storage depot. Curr Biol **16:** 1783–1795

Chisti Y (2013) Constraints to commercialization of algal fuels. J Biotechnol **167:** 201–214

Churchward MA, Brandman DM, Rogasevskaia T, Coorssen JR (2008) Copper (II) sulfate charring for high sensitivity on-plate fluorescent detection of lipids and sterols: Quantitative analyses of the composition of functional secretory vesicles. J Chem Biol **1:** 79–87

Correia I, Alonso-Monge R, Pla J (2010) MAPK cell-cycle regulation in *Saccharomyces cerevisiae* and *Candida albicans*. Future Microbiol **5:** 1125–1141

Criscuolo A, Zeller M, Cook K, Angelidou G, Fedorova M (2019) Rational selection of reverse phase columns for high throughput LC-MS lipidomics. Chem Phys Lipids **221:** 120–127

Dibrova DV, Galperin MY, Mulkidjanian AY (2010) Characterization of the N-ATPase, a distinct, laterally transferred Na^+-translocating form of the bacterial F-type membrane ATPase. Bioinformatics **26:** 1473–1476

Dubois M, Gilles KA, Hamilton JK, Rebers PA, Smith F (1956) Colorimetric method for determination of sugars and related substances. Anal Chem **28:** 350–356

Dunahay TG, Jarvis EE, Roessler PG (1995) Genetic transformation of the diatoms *Cyclotella cryptica* and *Navicula saprophila*. J Phycol **31:** 1004–1012

Eastmond PJ (2006) SUGAR-DEPENDENT1 encodes a patatin domain triacylglycerol lipase that initiates storage oil breakdown in germinating *Arabidopsis* seeds. Plant Cell **18:** 665–675

Fan J, Andre C, Xu C (2011) A chloroplast pathway for the de novo biosynthesis of triacylglycerol in *Chlamydomonas reinhardtii*. FEBS Lett **585:** 1985–1991

Goodson C, Roth R, Wang ZT, Goodenough U (2011) Structural correlates of cytoplasmic and chloroplast lipid body synthesis in *Chlamydomonas reinhardtii* and stimulation of lipid body production with acetate boost. Eukaryot Cell **10:** 1592–1606

Goold HD, Cuiné S, Légeret B, Liang Y, Brugière S, Auroy P, Javot H, Tardif M, Jones B, Beisson F, et al (2016) Saturating light induces sustained accumulation of oil in plastidal lipid droplets in *Chlamydomonas reinhardtii*. Plant Physiol **171:** 2406–2417

Graef M (2018) Lipid droplet-mediated lipid and protein homeostasis in budding yeast. FEBS Lett **592:** 1291–1303

Graham IA (2008) Seed storage oil mobilization. Annu Rev Plant Biol **59:** 115–142

Hagemann M (2011) Molecular biology of cyanobacterial salt acclimation. FEMS Microbiol Rev **35:** 87–123

Hakkila K, Antal T, Rehman AU, Kurkela J, Wada H, Vass I, Tyystjärvi E, Tyystjärvi T (2014) Oxidative stress and photoinhibition can be separated in the cyanobacterium *Synechocystis* sp. PCC 6803. Biochim Biophys Acta **1837:** 217–225

Harris EH (2001) *Chlamydomonas* as a model organism. Annu Rev Plant Physiol Plant Mol Biol **52:** 363–406

Herms A, Bosch M, Ariotti N, Reddy BJN, Fajardo A, Fernández-Vidal A, Alvarez-Guaita A, Fernández-Rojo MA, Rentero C, Tebar F, et al (2013) Cell-to-cell heterogeneity in lipid droplets suggests a mechanism to reduce lipotoxicity. Curr Biol **23:** 1489–1496

Hicks GR, Hironaka CM, Dauvillee D, Funke RP, D'Hulst C, Waffenschmidt S, Ball SG (2001) When simpler is better: Unicellular green algae for discovering new genes and functions in carbohydrate metabolism. Plant Physiol **127:** 1334–1338

Huang AHC (2018) Plant lipid droplets and their associated proteins: Potential for rapid advances. Plant Physiol **176:** 1894–1918

Ishida H, Yoshimoto K, Izumi M, Reisen D, Yano Y, Makino A, Ohsumi Y, Hanson MR, Mae T (2008) Mobilization of Rubisco and stroma-localized fluorescent proteins of chloroplasts to the vacuole by an ATG gene-dependent autophagic process. Plant Physiol **148:** 142–155

Jolivet P, Acevedo F, Boulard C, d'Andréa S, Faure JD, Kohli A, Nesi N, Valot B, Chardot T (2013) Crop seed oil bodies: From challenges in protein identification to an emerging picture of the oil body proteome. Proteomics **13:** 1836–1849

Kuroiwa T, Ohnuma M, Imoto Y, Kuroiwa H (2014) Lipid droplet formation in cells of the filamentous green alga *Klebsormidium nitens* as revealed by BODIOY-DiOC6 and BODIPY-nile red double-staining microscopy. Cytologia (Tokyo) **79:** 501–507

Lands WEM (1958) Metabolism of glycerolipides: A comparison of lecithin and triglyceride synthesis. J Biol Chem **231:** 883–888

Lands WE (2000) Stories about acyl chains. Biochim Biophys Acta **1483:** 1–14

Li X, Moellering ER, Liu B, Johnny C, Fedewa M, Sears BB, Kuo MH, Benning C (2012a) A galactoglycerolipid lipase is required for triacylglycerol accumulation and survival following nitrogen deprivation in *Chlamydomonas reinhardtii*. Plant Cell **24:** 4670–4686

Li Z, Thiel K, Thul PJ, Beller M, Kühnlein RP, Welte MA (2012b) Lipid droplets control the maternal histone supply of *Drosophila* embryos. Curr Biol **22:** 2104–2113

Lizaso A, Tan KT, Lee YH (2013) β-Adrenergic receptor-stimulated lipolysis requires the RAB7-mediated autolysosomal lipid degradation. Autophagy **9:** 1228–1243

Mansour MMF, Salama KHA, Allam HYH (2015) Role of the plasma membrane in saline conditions: Lipids and proteins. Bot Rev **81:** 416–451

Martin GJ, Hill DR, Olmstead IL, Bergamin A, Shears MJ, Dias DA, Kentish SE, Scales PJ, Botté CY, Callahan DL (2014) Lipid profile remodeling in response to nitrogen deprivation in the microalgae *Chlorella* sp. (Trebouxiophyceae) and *Nannochloropsis* sp. (Eustigmatophyceae). PLoS ONE **9:** e103389

Massey JB, Bick DH, Pownall HJ (1997) Spontaneous transfer of monoacyl amphiphiles between lipid and protein surfaces. Biophys J **72:** 1732–1743

Mastrobuoni G, Irgang S, Pietzke M, Assmus HE, Wenzel M, Schulze WX, Kempa S (2012) Proteome dynamics and early salt stress response of the photosynthetic organism *Chlamydomonas reinhardtii*. BMC Genomics **13:** 215

Miao XL, Li RX, Yao HY (2009) Effective acid-catalyzed transesterification for biodiesel production. Energy Convers Manage **50:** 2680–2684

Moellering ER, Benning C (2010) RNA interference silencing of a major lipid droplet protein affects lipid droplet size in *Chlamydomonas reinhardtii*. Eukaryot Cell **9:** 97–106

Moessinger C, Klizaite K, Steinhagen A, Philippou-Massier J, Shevchenko A, Hoch M, Ejsing CS, Thiele C (2014) Two different pathways of phosphatidylcholine synthesis, the Kennedy pathway and the Lands cycle, differentially regulate cellular triacylglycerol storage. BMC Cell Biol **15:** 43

Murphy DJ (1993) Structure, function and biogenesis of storage lipid bodies and oleosins in plants. Prog Lipid Res **32:** 247–280

Murphy DJ (2012) The dynamic roles of intracellular lipid droplets: From archaea to mammals. Protoplasma **249:** 541–585

Nguyen HM, Baudet M, Cuiné S, Adriano JM, Barthe D, Billon E, Bruley C, Beisson F, Peltier G, Ferro M, et al (2011) Proteomic profiling of oil bodies isolated from the unicellular green microalga *Chlamydomonas reinhardtii*: With focus on proteins involved in lipid metabolism. Proteomics **11:** 4266–4273

Noctor G, Foyer CH (1998) Ascorbate and glutathione: Keeping active oxygen under control. Annu Rev Plant Physiol Plant Mol Biol **49:** 249–279

Perrineau MM, Zelzion E, Gross J, Price DC, Boyd J, Bhattacharya D (2014) Evolution of salt tolerance in a laboratory reared population of *Chlamydomonas reinhardtii*. Environ Microbiol **16:** 1755–1766

Pulz O, Gross W (2004) Valuable products from biotechnology of microalgae. Appl Microbiol Biotechnol **65:** 635–648

Rambold AS, Cohen S, Lippincott-Schwartz J (2015) Fatty acid trafficking in starved cells: Regulation by lipid droplet lipolysis, autophagy, and mitochondrial fusion dynamics. Dev Cell **32:** 678–692

Rismani-Yazdi H, Haznedaroglu BZ, Hsin C, Peccia J (2012) Transcriptomic analysis of the oleaginous microalga *Neochloris oleoabundans* reveals metabolic insights into triacylglyceride accumulation. Biotechnol Biofuels **5:** 74

Rodríguez-Vargas S, Sánchez-García A, Martínez-Rivas JM, Prieto JA, Randez-Gil F (2007) Fluidization of membrane lipids enhances the tolerance of *Saccharomyces cerevisiae* to freezing and salt stress. Appl Environ Microbiol **73:** 110–116

Roesler K, Shintani D, Savage L, Boddupalli S, Ohlrogge J (1997) Targeting of the Arabidopsis homomeric acetyl-coenzyme A carboxylase to plastids of rapeseeds. Plant Physiol **113:** 75–81

Roomans GM (1999) Biological specimen preparation for transmission electron microscopy. Cell Biol Int **23:** 592

Schroeder B, Schulze RJ, Weller SG, Sletten AC, Casey CA, McNiven MA (2015) The small GTPase Rab7 as a central regulator of hepatocellular lipophagy. Hepatology **61:** 1896–1907

Shimizu T, Ohto T, Kita Y (2006) Cytosolic phospholipase A2: Biochemical properties and physiological roles. IUBMB Life **58:** 328–333

Shindou H, Shimizu T (2009) Acyl-CoA:lysophospholipid acyltransferases. J Biol Chem **284:** 1–5

Siaut M, Cuiné S, Cagnon C, Fessler B, Nguyen M, Carrier P, Beyly A, Beisson F, Triantaphylidès C, Li-Beisson Y, et al (2011) Oil accumulation in the model green alga *Chlamydomonas reinhardtii*: Characterization, variability between common laboratory strains and relationship with starch reserves. BMC Biotechnol **11:** 7

Sibi G, Shetty V, Mokashi K (2016) Enhanced lipid productivity approaches in microalgae as an alternate for fossil fuels: A review. J Energy Inst **89:** 330–334

Su J, Ye M, Lou Y, Yang Z, Sun T, Zhang R, Xu J, Zhou C, Yan X (2017) Low-molecular-mass organic acid and lipid responses of Isochrysis galbana Parke to high temperature stress during the entire growth stage. Algal Res **26:** 93–103

Takouridis SJ, Tribe DE, Gras SL, Martin GJO (2015) The selective breeding of the freshwater microalga *Chlamydomonas reinhardtii* for growth in salinity. Bioresour Technol **184:** 18–22

Tan KWM, Lee YK (2016) The dilemma for lipid productivity in green microalgae: Importance of substrate provision in improving oil yield without sacrificing growth. Biotechnol Biofuels **9:** 255

Tang D, Han W, Li P, Miao X, Zhong J (2011) CO_2 biofixation and fatty acid composition of *Scenedesmus obliquus* and *Chlorella pyrenoidosa* in response to different CO_2 levels. Bioresour Technol **102:** 3071–3076

Thompson GA Jr (1996) Lipids and membrane function in green algae. Biochim Biophys Acta **1302:** 17–45

Urzica EI, Vieler A, Hong-Hermesdorf A, Page MD, Casero D, Gallaher SD, Kropat J, Pellegrini M, Benning C, Merchant SS (2013) Remodeling of membrane lipids in iron-starved *Chlamydomonas*. J Biol Chem **288:** 30246–30258

Wada S, Ishida H, Izumi M, Yoshimoto K, Ohsumi Y, Mae T, Makino A (2009) Autophagy plays a role in chloroplast degradation during senescence in individually darkened leaves. Plant Physiol **149:** 885–893

Waku K, Nakazawa Y (1972) Acyltransferase activity to 1-acyl-, 1-O-alkenyl-, and 1-O-alkyl-glycero-3-phosphorylcholine in Ehrlich ascites tumor cells. J Biochem **72:** 495–497

Wältermann M, Steinbüchel A (2005) Neutral lipid bodies in prokaryotes: Recent insights into structure, formation, and relationship to eukaryotic lipid depots. J Bacteriol **187:** 3607–3619

Wang HL, Postier BL, Burnap RL (2002) Polymerase chain reaction-based mutageneses identify key transporters belonging to multigene families involved in Na^+ and pH homeostasis of *Synechocystis* sp. PCC 6803. Mol Microbiol **44:** 1493–1506

Welte MA (2007) Proteins under new management: Lipid droplets deliver. Trends Cell Biol **17:** 363–369

Welte MA, Gould AP (2017) Lipid droplet functions beyond energy storage. Biochim Biophys Acta **1862:** 1260–1272

Yamashita A, Sugiura T, Waku K (1997) Acyltransferases and transacylases involved in fatty acid remodeling of phospholipids and metabolism of bioactive lipids in mammalian cells. J Biochem **122:** 1–16

Yokthongwattana C, Mahong B, Roytrakul S, Phaonaklop N, Narangajavana J, Yokthongwattana K (2012) Proteomic analysis of salinity-stressed *Chlamydomonas reinhardtii* revealed differential suppression and induction of a large number of important housekeeping proteins. Planta **235:** 649–659

Zhu M, Zhou PP, Yu LJ (2002) Extraction of lipids from *Mortierella alpina* and enrichment of arachidonic acid from the fungal lipids. Bioresour Technol **84:** 93–95